Identification of the Ohmic-contact formation mechanism in the Au/Te/Au/GaAs system

K. Wuyts and G. Langouche
Instituut voor Kern- en Stralingsfysika, Katholieke Universiteit Leuven, B-3001 Leuven, Belgium

J. Watté, H. Vanderstraeten, and R. E. Silverans
Laboratorium voor Vaste Stof-fysika en Magnetisme, Katholieke Universiteit Leuven, B-3001 Leuven, Belgium

H. Münder, M. G. Berger, and H. Lüth
Institut für Schicht- und Ionentechnik (ISI), Forschungszentrum Jülich, D-5170 Jülich, Germany

M. Van Hove, H. Bender, and M. Van Rossum
Interuniversitair Micro Electronica Centrum (IMEC), B-3001 Leuven, Belgium
(Received 15 May 1991; revised manuscript received 5 February 1992)

The Ohmic-contact formation mechanism in furnace alloyed Au/Te/Au/(n-type GaAs) structures is investigated by the combined application of Mössbauer spectroscopy, x-ray diffraction, Raman scattering, and Auger-electron-spectroscopy depth profiling. A dominant shallow-donor-dopant behavior of the Te atoms (substitutional on As sites) can be questioned. The observed low-resistance conductivity is related to the presence of a (n^+-type Ga_2Te_3)/(n-type GaAs) heterojunction. Although the possibility of some residual n-type doping of the GaAs substrate remains, evidence is adduced that, in the Ohmic-contact formation mechanism, at least an equally important role is played by a degenerate As n-type doping of the Ga_2Te_3. Similar arguments are developed for the (Au-Ge)/(n-type GaAs) and Ge/Pd/(n-type GaAs) Ohmic-contact systems.

I. INTRODUCTION

Ohmic contacts on n-type GaAs have been extensively studied.[1] However, as the main line of research was directed towards device improvement, the contact formation mechanism is still under debate for most of the metallizations developed.[2] In particular both the Ge-based contacts, namely the Au-Ge device standard, and the recently developed Ge/Pd system, remain controversial.[2] So far, the discussion has mainly centered upon the question of whether the low-resistance conduction observed after alloying can be explained by a doping of the GaAs substrate, or by the formation of a graded crystalline or amorphous heterojunction.[2-4] The doping model requires the formation of a highly Ge-doped ($\simeq 2\times 10^{19}$ donors/cm^3) GaAs surface layer, over a width larger than the depletion depth (i.e., >60 Å), to permit electronic conduction to occur by quantum-mechanical tunneling.[2,5] The crystalline heterojunction model postulates the existence of a graded $Ge_x(GaAs)_{1-x}$ intermediate layer, the required grading width of which, however, being strongly dependent on the doping level of the GaAs substrate and of the Ge top layer.[3] According to this theory, the large barrier height at the metal-GaAs interface is divided into smaller metal-Ge and Ge-GaAs energy steps. The possibility of a defective regrown GaAs surface layer, causing Ohmic conduction according to the amorphous heterojunction model, has also been proposed.[2-4,6] This model requires the presence of a large density of localized gap states at the metal-semiconductor interface. The current transport through this contact layer is argued to occur by recombination, and/or by impurity-assisted tunneling or hopping of electrons between those localized defect levels.

To extend the study of the nature of n-type GaAs Ohmic contacts, a Te-based metallization scheme, with contact resistivities (r_c) comparable to those of the Au-Ge device standard, was developed by our research group.[7,8] The main models invoked to explain the Ohmic-contact formation in the Au-Ge/(n-type GaAs) system, can also be applied to the Au/Te/(n-type GaAs) contact. A highly n-type doped GaAs surface layer can be formed by the substitution of Te atoms on As lattice sites, forming a shallow-donor level. The role of Ge in the formation of a graded $(Ge)_x(GaAs)_{1-x}$ heterojunction can be taken over by the semiconducting compounds Ga_2Te_3 (having the zinc-blende lattice structure), and As_2Te_3, both having band gaps $E_g\simeq 1.0$ eV, and/or by elemental Te ($E_g=0.33$ eV). The observation that Te atoms also can form a deep level in GaAs (for instance, the Te_{As}-V_{Ga} defect complex[9,10]) on the other hand is compatible with the requirements of the amorphous heterojunction model.

In this paper, we report on an extensive investigation of the Au/Te Ohmic-contact scheme by the combined

application of Mössbauer spectroscopy, Raman scattering, x-ray diffraction (XRD), and Auger-electron-spectroscopy (AES) depth profiling, in correlation with electrical (*I-V*, and r_c) measurements. These data are interpreted by a reference study, including Mössbauer spectroscopy, XRD, optical (uv-ir) transmission and electrical measurements, of $(Au/As)_x(Ga_2Te_3)_{1-x}$ compounds. The results allow one to assign the observed low-resistance Ohmic conduction to the formation of a (Te/)Ga_2Te_3/GaAs crystalline heterojunction. It is argued that in this process a most crucial role is played by outdiffusing As, which provides a degenerate *n*-type doping of the Ga_2Te_3, leading to Fermi-level unpinning at the Ga_2Te_3/GaAs interface, and to the formation of an Ohmic metal/(Te/)Ga_2Te_3 contact. A similar concept is proposed to hold also for the Au-Ge/ and Ge/Pd/(*n*-type GaAs) systems.

II. EXPERIMENTAL PROCEDURES

Thin-film structures were prepared on (100)-oriented GaAs by resistive-heating evaporation of successively 50 Å Au, 500 Å Te, and 1200 Å Au in a vacuum of 10^{-6} Torr. A 200-nm-thick Si_3N_4 layer was deposited by plasma-enhanced chemical-vapor deposition (PECVD) on some of the samples before annealing. Prior to metallization, samples were etched in a [HCl]:[H_2O] (1:1) solution. Heat treatments (200–600 °C) were performed under a forming gas ambient (90% N_2+10% H_2) in a graphite strip heater ($t_{all}=15$ s) and in a conventional furnace ($t_{all}=3$ h).

Uniformly Si-doped (3×10^{17} at/cm^3) wafers were used for the electrical (*I-V*), and for some of the Raman measurements. *I-V* tests were also done on Zn (2×10^{18}/cm^3)-doped samples; semi-insulating (SI-) GaAs was taken in all other experiments. For the specific contact-resistivity measurements, an ion-implanted conducting channel was formed using 150-keV Si at a dose of 3×10^{13} atoms/cm^2. The contact resistivities of the samples were measured by a standard transmission line method. For the *I-V* measurements, wafers with pads 100×100 μm in size and gaps of 100 μm were prepared by photolithography; the data were acquired at room temperature and at 77 K.

To prepare samples containing Mössbauer probes, ^{129m}Te was implanted (40 keV) in the as-evaporated Te layer, after which the Au overlayer was deposited. The Mössbauer spectra were recorded at 4 K, using a 10-mg/cm^2 CuI absorber. With this absorber, having an effective thickness $t=7.13$, theoretically a minimum linewidth of 1.13(1) mm/s can be obtained. Taking into account geometrical and instrumental broadening, minimum linewidths of the order of 1.2–1.3 mm/s are expected.[11] θ-2θ XRD experiments were carried out on a computer-controlled Rigaku Dmax II rotating anode spectrometer. Cu $K\alpha$ radiation ($\lambda=1.541\,84$ Å) was selected with a flat pyrolitic graphite monochromator. ω scans were done by rocking the sample over a few degrees around a 2θ position. The Raman measurements were performed at room temperature using a triple spectrometer with multichannel detection (Dilor XY). Focus diameters of 2 and 100 μm were used. The spectra were taken in backscattering geometry with the 514- and 457-nm lines of an Ar^+ ion laser, and the 647-nm line of a Kr^+ ion laser, at an input power ≤1.0 mW. In these experiments different orientations for the polarizations of the incident and scattered light were used. The scattering configurations are indicated using the Porto notation.[12] For some measurements, the scattered light was detected without using an analyzer.

AES sputter depth profiles were recorded with a scanning Auger Microprobe (PHI 600) using a 10-keV, 0.03-μA, 45° incident electron beam with a spot size of 0.3 μm, by ion milling with a 1.5-keV, 1-μA/mm^2, 35° incident Ar^+ ion beam rastered over an area of 1.5×1.5 mm^2. The spectra were recorded with a 0.6% resolution and quantification was performed with the PHI sensitivity factors after correction for noise signals, but not for preferential sputtering and matrix effects. Using SiO_2 standards, and Rutherford backscattering spectroscopy reference spectra,[13] 1-min sputter time is calibrated as corresponding to 100(±10) Å. Auger mappings of the different elements were acquired at 10-keV with a 0.03-μA electron beam. A description of the preparation procedure of the Ga_2Te_3 reference powders can be found in Ref. 14.

III. RESULTS

A. Electrical measurements

Comparable specific contact resistivities ($\simeq5\times10^{-5}$ to 5×10^{-4} Ω cm^2) were measured on Au-Ge and Au/Te Ohmic contacts processed on identically prepared GaAs wafers.[7] These values were found to be independent of temperature in the 77–298 K range. Both metallization systems, however, differ by the alloy temperature at which the Ohmic conduction is observed. This onset of Ohmicity, which, for Ge contacts, commonly is reported to occur at 350–400 °C [after rapid thermal annealing (RTA)] was found at $\simeq$500 °C (RTA) for Te contacts with a 1200-Å-thick Au layer. The 350 °C (RTA) heat treatment yielded only a degradation of the Schottky characteristics: by *I-V* tests resistances (R) $\simeq10^3$–10^5 Ω were measured, which should be compared to values $\simeq10^6$–10^7 Ω found for as-deposited and low-temperature (300 °C) annealed contacts. For reference: the onset of Ohmicity as probed by these *I-V* measurements is defined to occur for resistance values ≤25 Ω ($r_c\simeq10^{-4}$–10^{-3} Ω cm^2).[13]

Apart from this shift in temperature for the Ohmicity onset, however, very similar traits in the alloy behavior of both types of contacts can be discerned. Indeed, similarly as reported for the Au-Ge metallization,[15] an increase in the contact resistivity by one to two orders of magnitude [$r_c\simeq(1-5)\times10^{-3}$ Ω cm^2] was observed for a 1200-Å Au/Te/Au/GaAs contact alloyed with a Si_3N_4 cap at 500 °C (RTA, capped). The contact resistivity decreased to lower values again [$\simeq(1-5)\times10^{-4}$ Ω cm^2], after a capped 550 °C anneal (RTA). Also, a reduction of the

amount of Au in the metallization shifted the temperature onset of Ohmicity to higher values: for a 700 Å Au/Te/Au/GaAs system alloyed without cap, Ohmic-contact characteristics were observed only after a 550 °C (RTA) anneal.[7] A similar feature was observed also for the Au-Ge contact.[15] Applying long-time thermal anneals (LTA), on the other hand, decreased the Ohmic-conductivity temperature: a 3 h, 400 °C [320 °C for Au-Ge (Ref. 15)] heat treatment resulted in similar resistances ($R \simeq 8-15\ \Omega$) as found at 500 °C (RTA). However, Schottky (or *p-n*, indiscernible with the analysis method used) characteristics were obtained on *p*-type GaAs substrates for all alloy conditions studied, a result which also conforms with the (Au-Ge)/(*p*-type GaAs) behavior,[16,17] but not with the results obtained by pulsed laser beam mixing of the Au/Te contacts.[9]

B. AES measurements

Figure 1 shows a scanning electron microscopy (SEM) micrograph of the surface of a (1200-Å Au)/(500-Å Te)/(50-Å) Au)/GaAs sample alloyed at 500 °C (RTA). An apparent inhomogeneity in the sample surface topography can be discerned: the surface is heavily subjected to the phenomenon of "balling," a feature reported also for the Au-Ge metallization.[1] Blisters, with dimensions of the order of micrometers, appear on the sample surfaces for anneal temperatures ≥ 350 °C. Microprobe AES depth profiling was applied to investigate the composition of the different surface features: results for 500 °C (RTA) contacts are shown in Fig. 2. Both the depth profiles of blisters, and of the sample surface in between were recorded. In the registered depth profiles, the oxygen trace was not included, which was done with the aim of decreasing the analysis time, in order to avoid sample drift during the measurement. By separate measurements, the oxygen signal was found peaked at the sample surface,[18] as reported also for alloyed Ni/Au/Te/Ni/GaAs structures.[13] In the depth profile of the as-deposited sample, however, a concentration of a few atomic percents of oxygen was observed only in the Te layer.[18]

The blisters, as can be seen on Fig. 2, consist mainly of Au [$\simeq$70(10) at. %] and Ga [$\simeq$20(5) at. %], with a very thin [$\simeq$50(30)-Å] Ga-Te layer on top. The spreads quoted correspond to the deviations found for different measurements on 500–550 °C samples (cf. also Ref. 18). From cross-sectional transmission electron microscopy (TEM) measurements, the total thickness of the blisters is estimated $\simeq$6000 Å, extending $\simeq$3000-Å deep into the GaAs substrate.[19] The AES depth profile taken in between the blisters reveals the formation of a rather thick layer, mainly composed of Ga and Te ($\simeq$10 at. % As is present at the surface) on top of the GaAs substrate. This finding is consistent with TEM analysis, which also indicated the presence of a surface layer with a different structure compared to the substrate, in between the blisters. Specimen preparation difficulties, however, excluded a further TEM investigation.[19] From the AES profiles, the thickness of this Ga-Te top layer for the 550 °C condition can be estimated to be $\simeq$160(30) Å; at 500 °C the thickness is $\simeq$220(40) Å; at 400 °C $\simeq$700(100) Å. However, at this 400 °C alloy temperature the separa-

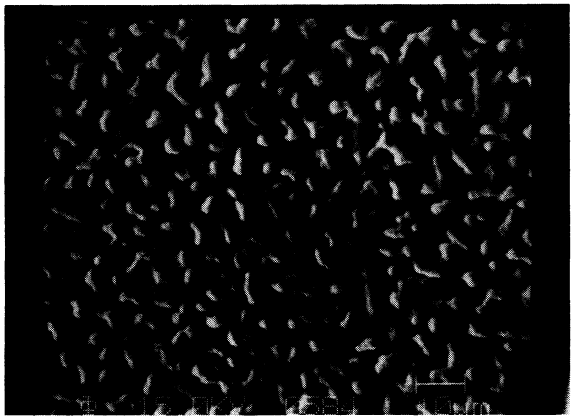

FIG. 1. SEM micrograph of the surface of a (1200-Å Au)/(500-Å Te)/(50-Å Au)/GaAs sample alloyed at 500 °C. The marker denotes a length of 10 μm.

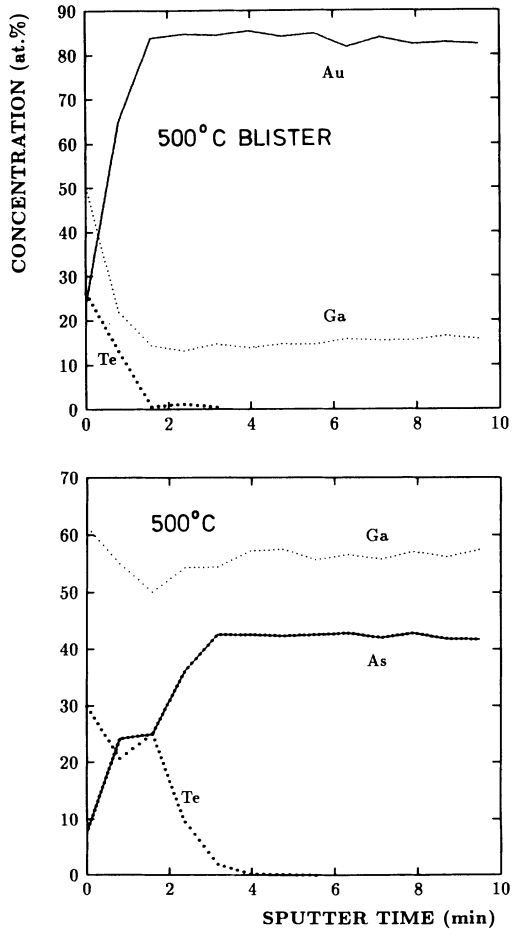

FIG. 2. AES depth profiles of the "normal surface" of a 500 °C annealed (1200-Å Au)/(500-Å Te)/(50-Å Au)/GaAs sample, and of a blister. 1 min sputter time is equal to 100 Å.

tion in between the Au-Ga islands is too small for obtaining clearly separated depth profiles. Hence, the amount of Au or As present in the Ga-Te parts of the surface layers cannot be quoted separately from the amount present in the blisters. At any rate, a rather high averaged surface concentration of As ($\simeq 1-5$ at.%) was found. Another difficulty in the interpretation of the AES results for all alloy conditions is the rather rough structure of the formed Ga-Te/GaAs interfaces: from TEM, a nonplanarity $\simeq 100$ Å can be deduced.[19] Hence, a precise determination of the composition and width of the Ga-Te layers, and especially of the Ga-Te/GaAs transition width, is not possible by sputter depth profiling.

C. Mössbauer measurements

As a first technique allowing one to probe the microscopic configuration of the Te atoms in the alloyed contact structures, ^{129}I Mössbauer spectroscopy (in the decay of ^{129m}Te) was applied. Data recorded from as-deposited and alloyed samples are presented in Fig. 3; the 550 °C spectrum was obtained after a Si_3N_4-capped annealing. All spectra, except the as-deposited (see below), were consistently fitted with only one component, with all parameters [isomer shift δ, quadrupole splitting $\Delta(eqQV_{zz}/h)$, asymmetry parameter η, and linewidth Γ] free; the results are listed in Table I. Due to the poor statistics of the spectra of the 500–550 °C uncapped annealed samples, by the evaporation of tellurium at this anneal stage, the corresponding fit quality is not quoted. The fit values given for the as-deposited, 400 °C (RTA), and 500–550 °C (RTA) conditions represent averages measured for three different processing runs. Deviations larger than the instrumental errors were found only for the quadrupole splitting; the spread observed is given in square brackets. In a fourth run a sample was annealed at 400 °C, one-half for 15 s, the other half for 3 h. This 400 °C (RTA) result is quoted separately [cf. Table I: (*)]. Reference data obtained from Ga_2Te_3, $As_2(Ga_2Te_3)_{19.6}$, and $Au_{5-17}(Ga_2Te_3)_{19-16.6}$ ^{129m}Te-labeled compounds are also included in the table; spectra are shown in Fig. 4. It should be kept in mind that the minimum linewidth that can be obtained with the absorber used is $\simeq 1.2-1.3$ mm/s (cf. the experimental procedures). Hence, one-component fits to the data yielding higher values indicate that the I nuclei in the sample investigated are subjected to a sum of different hyperfine fields.

For the as-deposited and 300 °C annealed samples, the hyperfine interaction parameters of ^{129}I in, respectively, Te and $AuTe_2$ were obtained.[20,21] Fits to the as-deposited tellurium spectra were improved by including a second set of parameters (fitted intensity $\simeq 9\%$) with the values fixed to those of orthorhombic TeO_2,[20] which is consistent with the indication, by the AES technique, of percents of oxygen in the as-evaporated tellurium layer. At 300 °C and higher alloy temperatures, traces of this TeO_2 contamination are no longer observable. Concerning the 300 °C spectrum, however, we should point out the large qualitative difference with the $AuTe_2$ spectrum reported in Ref. 21. As can be seen in Fig. 3, a very good fit, with a sufficiently narrow linewidth (1.3 mm/s) to our data was obtained with only one component, whereas a distribution of field gradients was necessary to fit the data reported in Ref. 21. This difference might be explained by the fact that the $AuTe_2$ formation in this Au/Te/Au

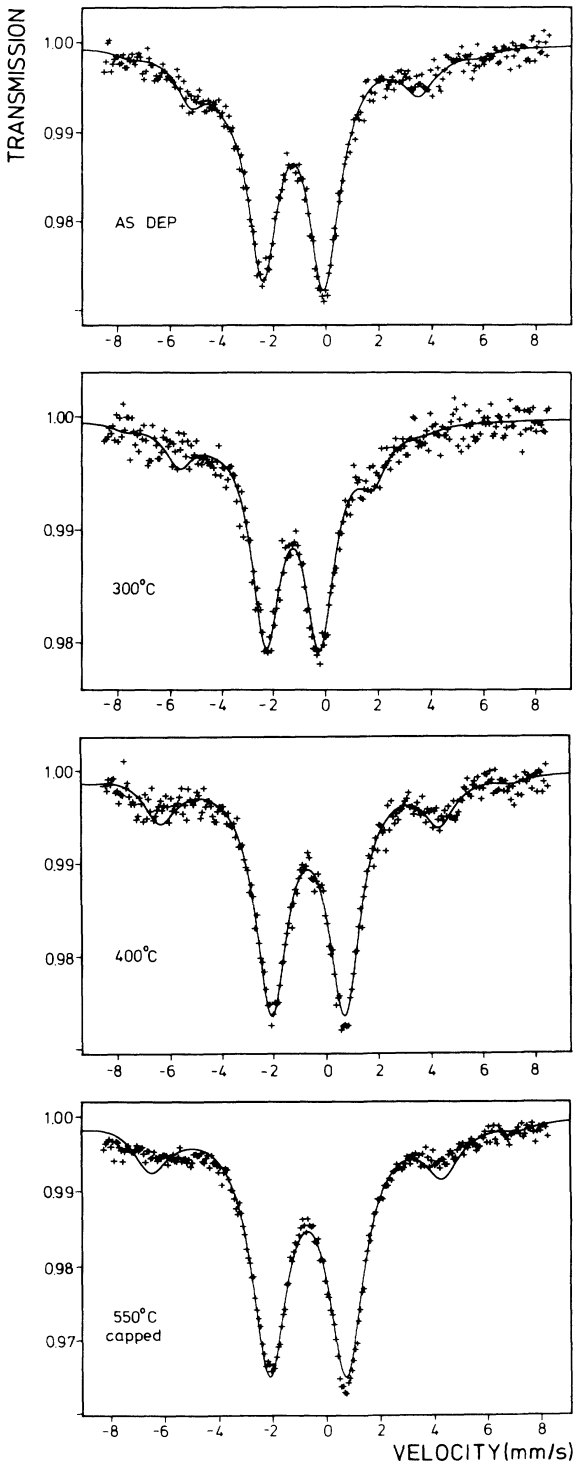

FIG. 3. ^{129}I Mössbauer spectra of as-deposited and alloyed (1200-Å Au)/[500-Å (^{129m}Te)/Te]/(50-Å Au)/GaAs structures, using a CuI absorber. Full lines represent one-component fits to the data, according to the parameter sets listed in Table I.

TABLE I. ^{129}I Mössbauer parameters of one-component fits to the spectra of alloyed Au/(^{129m}Te)Te/Au/GaAs contact structures, and of (Au/As)×[Ga_2(^{129m}Te)Te_3]$_{1-x}$ reference powders. The symbols δ, Δ, η, and Γ are defined in the text. Isomer shifts are absorber isomer shifts, given with respect to CuI. The spread observed is given in square brackets.

	δ (mm/s)	Δ (Mhz)	η	Γ (mm/s)	χ^2
Furnace-alloyed Au/Te/Au/GaAs					
as-dep.	+1.16(5)	−405(10	0.73(5)	1.3(1)	1.20[10]
300 °C (RTA)	+1.40(5)	+355(10)	0.60(5)	1.3(1)	1.27
400 °C (RTA)	+0.78(5)	+480[30]	0.87(5)	1.4(1)	1.45[25]
400 °C (RTA*)	+0.74(5)	+472(10)	0.84(5)	1.3(1)	1.29
400 °C (LTA)	+0.74(5)	+477(10)	0.83(5)	1.6(1)	1.62
500–550 °C (RTA)	+0.76(5)	+475[25]	0.80(5)	1.6(1)	
550 °C (RTA/capped)	+0.75(5)	+489(10)	0.83(5)	1.6(1)	3.41
$(Au/As)_x(Ga_2Te_3)_{1-x}$					
Ga_2Te_3	+0.70(5)	+477(10)	0.92(5)	1.8(1)	3.10
$As_2(Ga_2Te_3)_{19.6}$	+0.67(5)	+470(10)	0.95(5)	1.8(1)	3.26
$Au_5(Ga_2Te_3)_{19}$	+0.82(5)	+498(10)	0.86(5)	1.5(1)	1.35
$Au_{17}(Ga_2Te_3)_{16.6}$	+0.83(5)	+487(10)	0.84(5)	1.5(1)	1.15

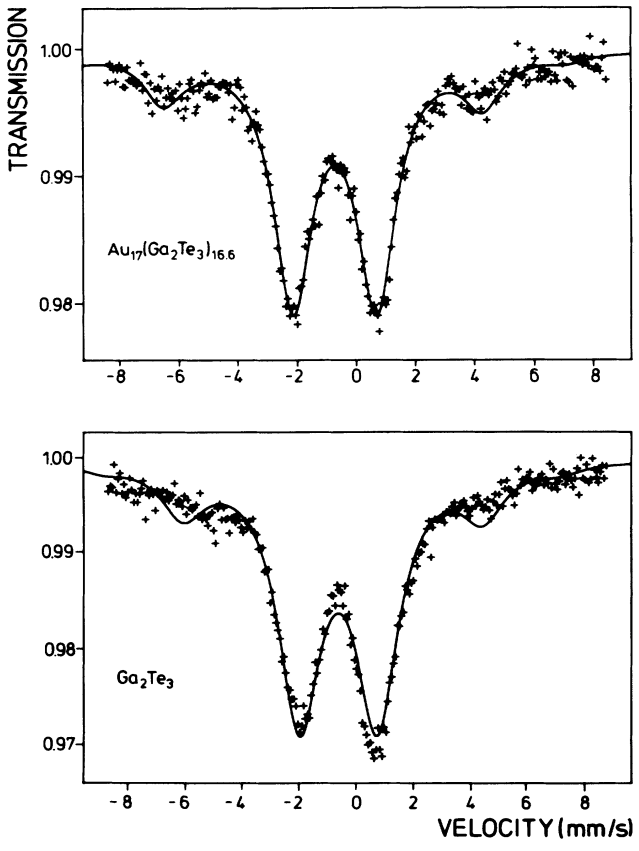

FIG. 4. ^{129}I Mössbauer spectra of ^{129m}Te labeled Ga_2Te_3 and $Au_{17}(Ga_2Te_3)_{16.6}$, using a CuI absorber. Full lines represent one-component fits to the data according to the parameter sets listed in Table I.

thin-film structure occurs by a solid-phase-reaction process,[7] whereas the $AuTe_2$ structure investigated in Ref. 21 was prepared starting from the molten phase.

The main interest of this paper, however, concerns the Ohmic, 500–550 °C (RTA) and 400 °C (LTA) contact structures, and actually, in view of the close resemblance in hyperfine parameters (δ, Δ, and η), the characterization of their difference with the non-Ohmic 400 °C (RTA) samples. As can be seen in Table I, the parameters fitted to these high-temperature (400–500 °C) spectra correspond well to either Ga_2Te_3 [indistinguishable from $As_2(Ga_2Te_3)_{19.6}$] or $Au_{17}(Ga_2Te_3)_{16.6}$. The main difference between the latter spectra is the increased (fitted) linewidth in the transition from Au-alloyed to pure Ga_2Te_3, and the corresponding decrease in fit quality (increase of the χ^2 value) of the one-component fit. This misfit is predominantly related to the big asymmetry between the two main peaks, and to the missing sidewings in the experimental data (cf. Fig. 4). The same differences can be observed between the non-Ohmic, 400 °C (RTA), and Ohmic, 400 °C (LTA), and 500–550 °C (RTA) annealed Au/Te/Au/GaAs structures. The fitted (one-component) linewidth increases from 1.3(1) and 1.4(1) mm/s for the 400 °C (RTA) spectra to 1.6(1) mm/s for the 400 °C (LTA) and 550 °C (RTA) data. Also, a more pronounced deviation between the one-component fits and the experimental data appears; as can be seen for the 550 °C (RTA, capped) spectrum shown (Fig. 3), the asymmetry between the spectral main lines is not reproduced and the smaller sidewings are missing. Thus, from this Mössbauer analysis we can conclude that the transition to Ohmic-type conductivity in alloyed Au/Te/Au/GaAs structures is correlated to a change in the preferential binding of the Te atoms from Au-rich Ga_2Te_3, tentatively

identified as $AuGa_2Te_3$ (see the discussion), to pure or As-doped Ga_2Te_3.

No evidence for the substitution of Te atoms on As sites, forming a highly doped GaAs surface layer, could be deduced from the Mössbauer data. Fits to the 500–550 °C (RTA, with and without Si_3N_4 cap), and 400 °C (LTA) spectra including the parameter set associated with this shallow donor defect [$\delta = 0.70(5)$ mm/s, $\Delta = 0$] (Ref. 22) yielded as a result a zero (at least within the detection limits of the Mössbauer technique, i.e., fractions $\geq 1\%$ of the total amount of Mössbauer probes) occupation of this lattice site. Evidence of the formation of a $Te_{As}{}^{-}V_{Ga}$ defect complex in the GaAs surface layers as a result of the alloy procedure, was deduced from Mössbauer spectra in a previous paper.[8] This interpretation, however, should be questioned since the fitted intensity of the corresponding hyperfine set did not surpass its percentual contribution expected for being one of the components of the Ga_2Te_3 spectrum.[10] In a last remark, we wish to point out that when a set of hyperfine parameters fixed on the values of elemental tellurium was included in fits to the 500–550 °C spectra, its intensity increased to $\simeq 2$–6% of the total Mössbauer resonance. This result should be interpreted as indicating that for these alloy temperatures the presence of some elemental Te in the contact structures is not excluded. For the 400 °C (RTA), and 550 °C (RTA, capped) alloy conditions, this Te contribution was fitted to a zero intensity.

D. XRD measurements

XRD measurements were performed on as-deposited, 400 °C (RTA and LTA), and 500–550 °C (RTA and RTA/capped) annealed Au/Te/Au/GaAs structures; spectra, with ω scans in the insets, are shown in Fig. 5. The presence of Ga_2Te_3 crystallites in the alloyed-contact structures is clearly confirmed: the diffraction peaks labeled b/b' in the figure correspond to the (200) and (400) lattice planes of Ga_2Te_3, or closely related compounds. One can, however, note that of the full x-ray profile of Ga_2Te_3, only the signals arising from the (200) and (400) planes are apparent, which gives a first indication for a preferential orientation of these Ga_2Te_3 crystallites with respect to the GaAs substrate. In Table II, an analysis of these Ga_2Te_3 peaks, together with the relevant part of the data measured on Ga_2Te_3, Au_{5-17} $(Ga_2Te_3)_{19-16.6}$, and $As_1(Ga_2Te_3)_{19.8}$ reference powders, is summarized. The lattice constants d of the different compounds were calculated as $d = \lambda/(\sin\theta_{400} - \sin\theta_{200})$. Also tabulated is the integrated intensity ratio between the corresponding peaks, and for the alloyed Au/Te/Au/GaAs samples the full width at half maximum (FWHM) of the ω scans taken around these angles (cf. Fig. 5); the instrumental broadening of the experimental setup accounts for values $\simeq 0.10(1)°$. The FWHM values observed are sufficiently small to allow for concluding that an epitaxial growth of Ga_2Te_3 on the GaAs substrate occurred.

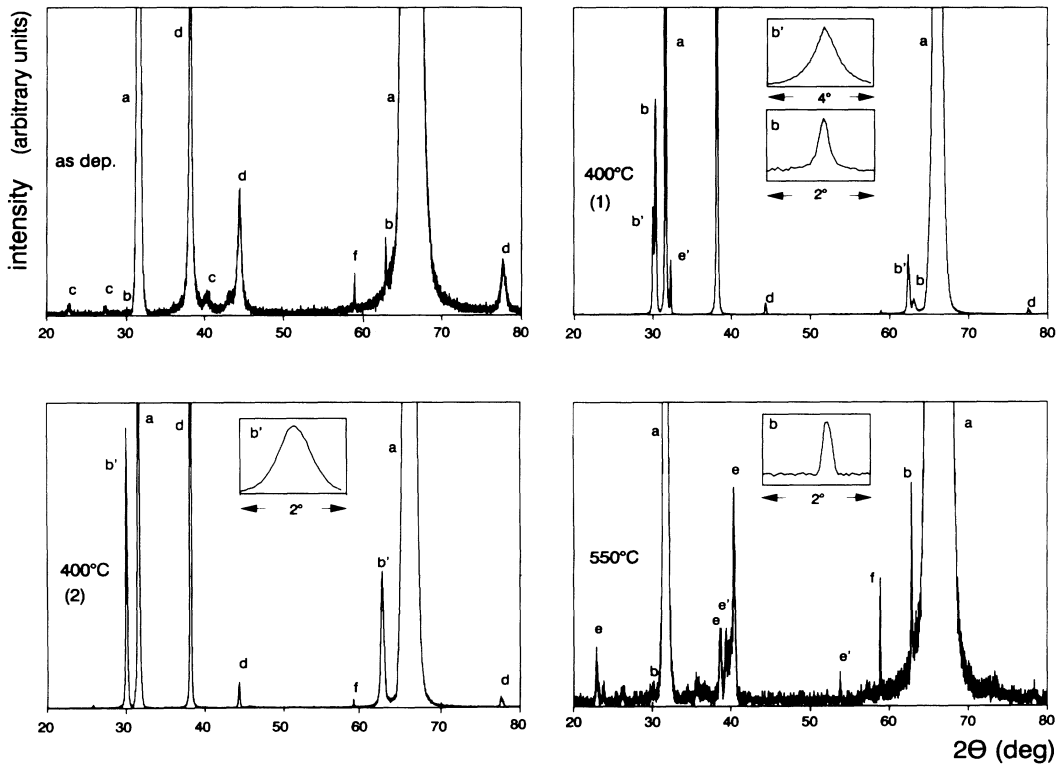

FIG. 5. X-ray profiles of as-deposited and alloyed (1200-Å Au)/(500-Å Te)/(50-Å Au)/GaAs structures. Peaks labeled a correspond to GaAs, $b/b' = Ga_2Te_3/AuGa_2Te_3$, c = Te, d = Au, $e/e' = Au_{0.79}Ga_{0.21}/Au_2Ga$, and f = As. In the insets, ω scans about the Ga_2Te_3 (400) reflection are shown.

Definite changes are found in the structure of the Ga_2Te_3-related compounds for the different alloy conditions. These x-ray results can, similarly as concluded from the Mössbauer data, be correlated (at least partly, see further) to the changes observed in the structure of $Au_x(Ga_2Te_3)_{1-x}$ reference powders: with increasing Au concentration, an increase in the (100) planes spacing is seen. A value of 5.979 Å for $Au_{17}(Ga_2Te_3)_{16.6}$, or $AuGa_2Te_3$, compared to 5.904 Å for pure Ga_2Te_3 is found. This lattice expansion is accompanied by a strong decrease in the (200) compared to the (400) peak intensity (a 1.4:1 ratio opposed to 6.2:1). The x-ray spectrum of 1 at. % As-doped Ga_2Te_3, on the other hand, is indistinguishable of that of pure Ga_2Te_3.

Similar transitions occur in the alloyed Au/Te/Au/GaAs structures. At 400 °C (RTA), though clearly both types of compounds, $AuGa_2Te_3$ and Ga_2Te_3, are formed [cf. measurement (1), Fig. 5 and Table II], a more dominant presence of the Au-rich crystallites is indicated. The 5.920-Å spacing and 1.3:1 intensity ratio obtained in the averaged [compared to (1)] measurement (2) are closer to the 5.944-Å and 1.1:1 values observed for the Au-rich variant compared to these (5.881 Å/6.8:1) for the pure (or As-doped) Ga_2Te_3. Note also that the observed intensity ratios of the $AuGa_2Te_3$ and Ga_2Te_3 associated x-ray peaks in measurement (1) do not reflect the right relative abundance of the different compounds. At least, in such an evaluation one should take into account the different widths of the corresponding ω scans: a FWHM of 0.22° namely was measured for the 5.881-Å/6.8:1 Ga_2Te_3, whereas a value of 1.02° was found for the 5.944-Å/1.1:1 Au-Ga_2Te_3 (Table II). However, an increase in alloy temperatures to 500 °C (RTA) and 550 °C (RTA, capped), respectively, results in a more dominant (possibly As-doped) Ga_2Te_3 regrowth (see Table II). For the 550 °C (RTA) and 400 °C (LTA) alloy conditions, a third Ga_2Te_3 variant is formed, characterized by approximately a 0.1:1 (200):(400) peak intensity ratio, and grown (almost) perfectly epitaxial on the GaAs substrate, as can be deduced from the $\simeq 0.15°$ widths of the rocking curves. The observation of this small rocking width allows for a labeling of this third Ga_2Te_3 variant as a pseudomorphic (on GaAs) Ga_2Te_3 phase. It is not excluded that this pseudomorphic phase should be identified as a $(GaAs)_{1-x}(Ga_2Te_3)_x$ $(x > 0.3)$ compound reported to exist in bulk form.[23] Definite evidence so far is currently lacking. At least, the lattice constants indicated for this phase (5.72–5.77 Å) (Ref. 23) can indeed allow for a strained growth of the $\simeq 160-$Å-thick layer (cf. the AES section). Note that the $d = 5.893-5.895$-Å values listed in Table II for this pseudomorphic phase, correspond to the strained lattice spacing, as in the detection geometry used, only the planes parallel to the surface are measured.

Apart from this Ga_2Te_3 formation, the XRD measure-

TABLE II. Lattice constant d, and intensity ratio of the (200) and (400) peaks of $(Au/As)_x(Ga_2Te_3)_{1-x}$ reference powders, and of related compounds observed in alloyed Au/Te/Au/GaAs structures. Also tabulated for the contact structures is the width of the ω scans taken around these peaks.

	d (Å)	I_{200}:I_{400}	FWHM (ω scan)
Furnace-alloyed Au/Te/Au/GaAs			
(1)400 °C (RTA)	5.944(10)	1.1:1[±15%]	1.02(1)°
	5.881(10)	6.8:1[±15%]	0.23(1)°
(2)400 °C (RTA)	5.920(10)	1.3:1[±15%]	0.75(1)°
400 °C (LTA)	5.893(10)	0.07:1[±15%]	0.15(1)°
500 °C (RTA)	5.899(10)	3.2:1[±15%]	0.44(1)°
550 °C (RTA)	5.895(10)	0.13:1[±15%]	0.16(1)°
550 °C (RTA/capped)	5.898(10)	2.5:1[±15%]	0.70(1)°
$(Au/As)_x(Ga_2Te_3)_{1-x}$			
Ga_2Te_3			
Tabulated	5.899	3.8:1	
measured	5.904(10)	6.2:1[±15%]	
$As_1(Ga_2Te_3)_{19.8}$			
	5.908(10)	4.2:1[±15%]	
$Au_5(Ga_2Te_3)_{19}$			
	5.932(10)	5.0:1[±15%]	
$Au_{17}(Ga_2Te_3)_{16.6}$			
	5.979(10)	1.4:1[±15%]	

ments also indicate a gradual consumption of the elemental Au [still present in the 400 °C (RTA) spectra] in Au_xGa_y phases, with most dominantly a $Au_{0.79}Ga_{0.21}$ alloy, whose composition corresponds to the one deduced for the surface blisters (cf. the AES section). Also for these compounds, a highly textured orientation with respect to the substrate was found. The presence of elemental Te in a 500 °C (RTA) sample, as reported previously,[8] was not confirmed in any of the measurements on the high-temperature (≥ 500 °C) or long-time (≥ 3-h) annealed structures. However, due to the overlap of some of the Te peaks with those of $Au_{0.79}Ga_{0.21}$, the sensitivity factor of the XRD technique in detecting Te crystallites is strongly reduced (cf. the difference between the signal of a $\simeq 500$-Å-thick Te layer with that of 1200-Å Au in the as-deposited spectrum). Hence, the presence of elemental Te, dispersed, for instance, in $\simeq$ micrometer-sized islands a few tens of Å thick cannot be excluded. On the other hand, in the as-deposited XRD spectrum, besides the elemental Te signals, the presence of minor amounts of pseudomorphic Ga_2Te_3, and of elemental As, can also be noticed, whose phases probably are formed by a reaction between the substrate constituents and the impinging Te atoms during deposition.

E. Raman measurements

Raman spectra were taken from 500–550 °C (RTA) alloyed Au-Te contacts processed on semi-insulating (Fig. 6: $\lambda = 514$ nm, unpolarized detection), and on *n*-type GaAs substrates (Figs. 7 and 8: $\lambda = 457$ nm, polarized detection). For reference, the spectra of Ga_2Te_3, Te, and $\simeq [1.7(3)] \times 10^{19}/cm^3$ Si-doped, thin (17–100 nm) GaAs layers grown by molecular beam epitaxy (MBE) were acquired. This $[1.7(3)] \times 10^{19}/cm^3$ doping level was deduced from Hall-effect measurements on the thickest (100-nm)-grown layer, and could be obtained due to the use of off-equilibrium GaAs growth conditions, namely, by reducing the GaAs growth temperature to lower values (≤ 400 °C), and by the supply of an excess of Ga atoms.[24]

The data shown in Fig. 6 were obtained with a laser-light focus diameter of 2 μm. Here, the structure of the annealed Au/Te/Au/GaAs contacts was probed at different locations between the AuGa islands. From these spectra, the presence of elemental Te and Ga_2Te_3 in the alloyed contact structures can clearly be deduced. The absence of the substrate signal at those spots (fewer in number) for which the Te signal dominates the spectrum can be understood if one takes into account the smaller band gap of Te ($E_g = 0.33$ eV) compared to that of Ga_2Te_3 ($E_g = 1.0$ eV), yielding a more reduced light penetration depth (d) for the former ($d = 10$ nm) compared to the latter ($d = 50$ nm) semiconductor. This difference also explains the dominance of the Te peaks in the spectra compared to their corresponding intensity (or absence) in the Mössbauer and x-ray scans.

The lines appearing at $\simeq 292(1)$ cm^{-1} (Figs. 6, 7, and 8) are the GaAs LO-phonon modes. The peaks at 269 cm^{-1} could correspond to the GaAs TO lattice vibration, or to the L^- mode of the coupled plasmon LO-phonon (PLP) modes, which can be observed in highly ($\geq 10^{16}$ donors/cm^3) doped GaAs.[25] For concentrations $\geq 5 \times 10^{17}$ donors/cm^3, the L^+-mode signal also appears, clearly separated in position from the LO phonon.[25] At these doping levels, namely, the free-carrier plasma frequency becomes comparable to the frequency of the optical phonons. The plasmons interact with the LO pho-

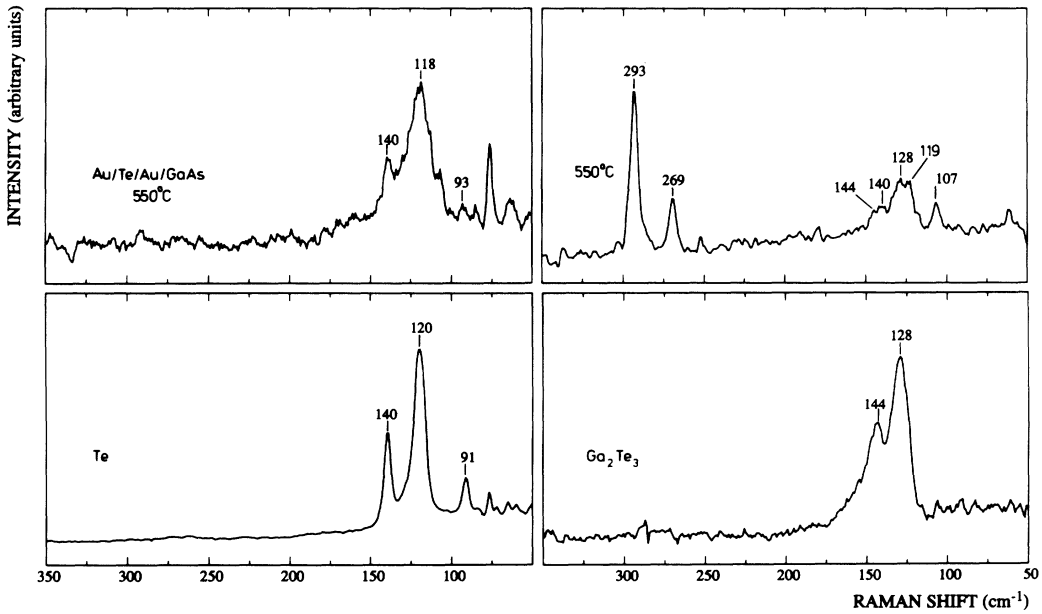

FIG. 6. Raman spectra of (1200-Å Au)/(500-Å Te)/(50-Å Au)/GaAs structures annealed at 550 °C, probed at different locations on the sample surface, and reference spectra of Te and Ga_2Te_3. The probe wavelength $\lambda = 514$ nm, the scattered light was detected without using an analyzer.

nons via their electrical fields and cease to be independent excitations of the system. This, then, gives rise to two coupled modes L^- and L^+ (cf. Fig. 8). Hence, in the case that the 269-cm^{-1} line is due to an L^- mode arising from the presence of a high density of free carriers in the GaAs surface layers, the corresponding high-frequency L^+ mode should be observed with a frequency depending on the free-carrier concentration.[25] However, as shown in Fig. 7 (with the wave-number scale displayed up to 1200 cm^{-1}), in the spectral range 300–2000 cm^{-1} no PLP mode was observed, not even with a 647-nm laser wavelength probe, which allows for an investigation of the deeper GaAs layers. This result provides a first argument for attributing the 269-cm^{-1} line to a GaAs TO lattice vibration. Conclusive evidence concerning this dichotomy, however, is given by taking the different symmetry selection rules of phonons and PLP modes into account. An L^- mode close to the TO phonon frequency of GaAs obeys the same symmetry selection rules as the LO phonon and will give a contribution only in the symmetry-allowed scattering configuration $z(xy)\bar{z}$ [Fig. 7(b)]. As can be seen in Fig. 7(c), the 269-cm^{-1} signal clearly remains in the $z(yy)\bar{z}$, the LO/L^--forbidden configuration, which gives most definite evidence for its labeling as a TO phonon. The appearance of this rather strong TO mode in the spectra indicates the presence of disorder or of defects in the GaAs surface layers, most probably resulting from the regrowth of a thin interfacial layer of GaAs as a result of the alloy process. The only phonon mode which should be observed from a GaAs(100) surface in backscattering geometry, namely, is the LO-phonon mode; the presence of defects can relax the selection rules allowing for the observation of the TO mode.[26]

To find out the sensitivity of the Raman technique in excluding any doping of the substrate due to the alloy procedure, measurements were performed on thin heavily doped GaAs layers; spectra are shown in Fig. 8. As mentioned above, from Hall-effect measurements the doping level in these layers was characterized to be of the order of $[1.7(3)]\times10^{19}$/cm^3. From the position of the L^+ mode in the corresponding Raman spectra, a doping level of $[1.3(1)]\times10^{19}$/cm^3 is deduced for the 100-nm n^+-type GaAs layer, and of 8×10^{18}/cm^3 for the 30- and 17-nm-thick layers. This apparent free-carrier-density lowering for the thinner grown layers most probably can be attributed to the surface and interface depletion-depth corrections. For a 1.4×10^{19}/cm^3 doping level, namely, the total depletion depth ($w_{tot}=w_{interface}+w_{surface}$) equals 16 nm.[27] Hence, the thickness of the free-carrier-containing layer should be equal to 1 nm. Taking into account free-electron leakage of a few Debye lengths into the depletion region,[27] the observation of a resulting, averaged 8×10^{18}/cm^3 doping level can be thought plausible. Accordingly, for the maximum free-carrier-layer thickness probed on the 17-nm wafer, a value ≤ 5 nm can be set. From the fact that this structure still yields a clearly detectable Raman signal (cf. Fig. 8), the formation of a similar layer formed in the alloyed Au/Te/Au/GaAs structures should be observable by Raman spectroscopy. Referring to the discussion of these spectra, conducted above, its presence clearly can be denied.

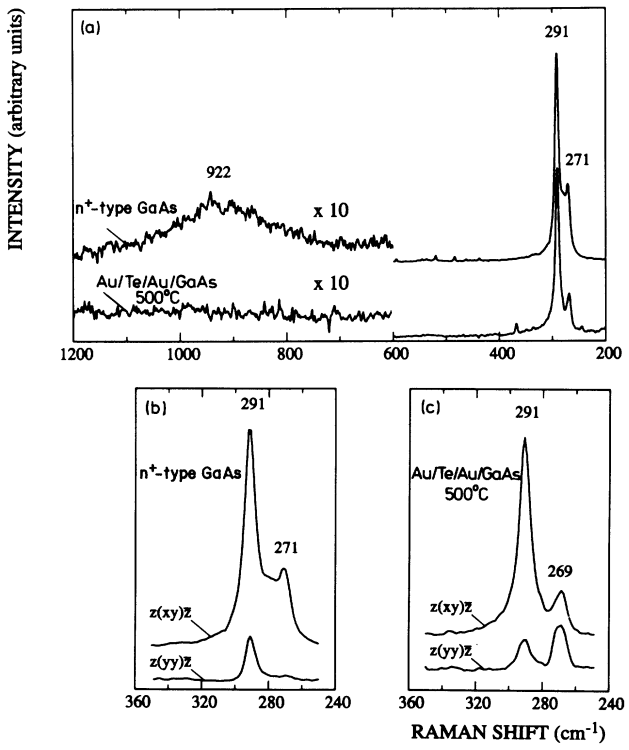

FIG. 7. Raman spectra of a 30-nm (n^+-type GaAs)/(SI-GaAs) structure [(a) and (b)], and of a (1200-Å Au)/(500-Å Te)/(50-Å Au)/GaAs sample [(a) and (c)] annealed at 500 °C. In (b) and (c), different orientations for the polarizations of the incident and scattered light are used. The 922-cm^{-1} peak position of the L^+ mode (n^+-type GaAs) corresponds to a doping level $\simeq 8\times10^{18}$ donors/cm^3. The probe wavelength $\lambda=457$ nm.

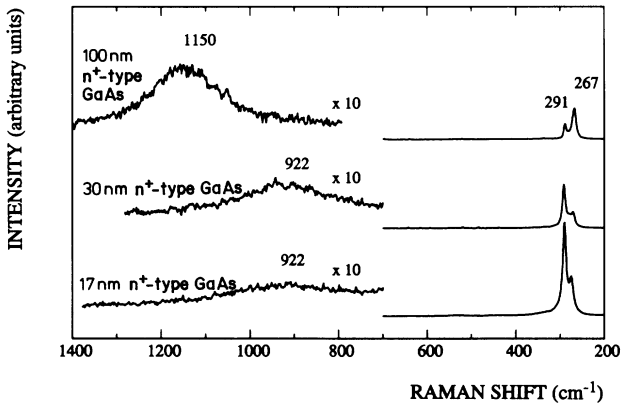

FIG. 8. Raman spectra of 100-, 30-, and 17-nm n^+-type GaAs, grown by MBE on SI substrates. The 1150-cm^{-1} and 922-cm^{-1} peak positions of the L^+ mode correspond to doping levels of 1.3×10^{19} and of 8×10^{18} donors/cm^3, respectively. Also, the L^- (267–271-cm^{-1}) mode, and the LO-phonon mode from the depletion layer are observed. The probe wavelength $\lambda=457$ nm.

IV. DISCUSSION AND CONCLUSIONS

In the first paragraph of this concluding section, we will develop a consistent picture of the metallurgical processes occurring during the high-temperature ($\geq 350\,^{\circ}C$) alloying of the Au/Te/Au/GaAs contact structures. The main part of this section is devoted to a discussion of the Ohmic-contact formation mechanism in this system, namely whether the doping model or the graded crystalline or amorphous heterojunction model is most appropriate (cf. the Introduction). In a last note, the possible relevance of this Au/Te research for the more intensively used Au-Ge and Ge/Pd contact schemes is treated.

From the information adduced by the SEM, TEM, and AES measurements, the occurrence of a liquid-phase process as a result of the high-temperature alloying can be concluded. The formation of the Au-Ga dropletlike surface structures, and the presence of rough, nonplanar interfaces is consistent with this hypothesis. Another indication of melting is the coincidence of the appearance of these surface blisters with the crossing of the Au-Ga eutectic temperature (341 °C). Hence, in agreement with previous investigations of the Au-GaAs and (Au-Ge)-GaAs interactions,[28,29] it can be proposed that this melting process is initiated by the melting of an Au-rich Au-Ga solid solution. As a result, during the cooling down of the system, a segregated growth of Au-Ga and of Ga-Te phases takes place. This model also is consistent with the observed increase of the onset of Ohmicity temperature with a decreasing Au-thickness. The metallurgical processes leading to the formation of the (Au/Te)-GaAs Ohmic-contact structure, namely, can be thought to be initiated by the Au-GaAs melting. Hence, the observed time- and temperature scale of the (Au/Te)-GaAs onset of Ohmicity can be assumed to be related to the extent of the Au-GaAs interdiffusion behavior, which is determined by the amount of Au present, and by the alloy temperature and time.

Most crucial in the Ohmic-contact formation process are the lattice sites occupied by the Te atoms after alloying. A most dominant Te *n*-type doping of the GaAs (Te atoms substitutional on As sites) can be excluded. Both Mössbauer and Raman spectroscopy were proven to be very sensitive in probing the substitution of Te dopants on electrically active sites in GaAs, the former by the observation of Te atoms on a regular (substitutional) lattice site,[22] the latter by the direct evaluation of carrier concentrations $\geq 5\times 10^{17}$ donors/cm^3 by the coupled plasmon LO-phonon modes.[25] However, no sign of these features is present in our spectra. Some doubt in excluding a dopant behavior of part of the Te atoms probably might remain from the analysis of the Mössbauer data, since the detection (fitting) of a fraction representing $\leq 1\%$ of the total amount of Mössbauer probes is questionable. The Raman technique, however, was proven to be sensitive to the presence of very thin highly doped GaAs layers: MBE-grown *n*-doped GaAs with a free-carrier layer extended over a thickness $\simeq 1-5$ nm still yielded a clearly detectable signal. Hence, the formation of a high free-carrier-density GaAs surface or intermediate layer, as a result of the alloy procedures used, can be denied, or at least is highly questionable.

As mentioned above, as a most dominant Te-related feature, the formation of a Ga-Te layer on top of the GaAs substrate can be deduced. From the combined application of Mössbauer, XRD, Raman, and AES measurements on Ohmic ($T_{all}\geq 500\,^{\circ}C$, $t_{all}=15$ s; $T_{all}=400\,^{\circ}C$, $t_{all}\geq 3$ h) contacts, the structure of this Ga-Te top layer was characterized as a Ga_2Te_3/GaAs heterojunction. This observation fits in the graded crystalline heterojunction model, and might even be the clue for understanding the Ohmic-contact formation mechanism, provided definite answers can be given concerning the exclusion of the other (doping and amorphous heterojunction) models, and provided the non-Ohmic behavior as a result of lower-temperature (400 °C), short-time, annealing cycles can be explained. The Te-GaAs doping model was (partly) argued upon above. However, although the presence of a high free-carrier density as a result of the alloy procedures used can be excluded, the possibility remains that a highly doped region may lie within the Ga_2Te_3/GaAs interface depletion region. By this, we mean that due to some residual Te *n*-type dopant behavior (for instance, $\simeq 10^{18}$/cm^3 over a few nanometers), the GaAs depletion width might be reduced, resulting in a thinner barrier to electron transport across the Ga_2Te_3/GaAs junction. Consistent with this hypothesis is the observation of a disorder-activated TO phonon in the Raman measurements, which might indicate the presence of a thin regrown interfacial layer of GaAs incorporating Te as an *n*-type dopant. However, in view of the structure of the contacts, this increased GaAs doping alone cannot explain the Au/Te-GaAs Ohmic-contact formation mechanism. AES analysis namely showed a complete coverage of the GaAs substrate by AuGa blisters and by the Ga-Te phases. Hence, the main questions regarding the observed Ohmicity, at least should include the problem of the conductivity through the Ga-Te [(Te/)Ga_2Te_3] top layer, and its contactibility both at the probe metal-Ga_2Te_3 interface, and the Ga_2Te_3/GaAs interface.

Kirillov and Chung,[4] suggested for alloyed (Au-Ge)-GaAs contact structures, a conduction mechanism according to the amorphous heterojunction model; a resonant tunneling process assisted by deep impurity levels in a graded Ge-GaAs heterojunction was proposed. However, although the formation of a Ga_2Te_3/GaAs heterostructure is observed for the Au/Te-GaAs contact, only minor evidence in favor of a similar conduction mechanism can be deduced from our measurements. Mössbauer spectra of the Ohmic-contact structures can adequately be fitted (not shown) with only the components (and corresponding intensity) constituting the $AuGa_2Te_3$, and Ga_2Te_3 spectra[10,30]; no indication for any abundant presence of Te-defect levels is found. Raman scans, on the other hand, consistently show a GaAs-disorder-activated TO phonon, its intensity and shape, however, being far from the amorphous GaAs features observed after pulsed-laser-beam mixing of the contacts.[12] This processing method yielded similar low resistivities on *p*-type and *n*-type GaAs with, correlated to this electrical contact behavior, the formation of a high

density of $Te_{As}{}^{-}V_{Ga}$ defect complexes, as probed by Mössbauer spectroscopy.[9,10] Based on these observations, conduction in these laser-alloyed structures was argued to occur according to the amorphous heterojunction model.[9,10,12] However, as with furnace alloying, rectifying characteristics were obtained on *p*-type substrates; the contribution of the Raman-indicated defect levels to the low-resistance conductivity observed for furnace-alloyed Au/Te/Au/(*n*-type GaAs) samples, investigated in this paper, can be assumed not to be dominant.

On the contrary, a consistent interpretation of the Ohmic-contact behavior of furnace-alloyed Au/Te-GaAs contacts can be developed based on the presence of arsenic in the Ga_2Te_3 top layer, as indicated by AES depth profiling. It has been shown by the combined application of optical (uv-ir) transmission and electrical measurements that arsenic acts as an *n*-type dopant in Ga_2Te_3.[30] For a doping level $\simeq 7.10^{19}$ As atoms/cm^3 temperature-independent (77–293 K) Ohmic-contact characteristics were observed on Ga_2Te_3 reference structures, even when the semiconductor surface was probed directly without any intermediate metallization step.[30] A similar degenerate doping of the Ga_2Te_3 top layer, formed after alloying of the Au/Te/Au/GaAs contact structures, can be expected for the high concentrations ($\simeq$ atomic percents) of arsenic detected. An Ohmic-behaving metal-Ga_2Te_3 contact barrier, and a low-resistance conductivity through the Ga_2Te_3 layer, correspondingly, can be assumed. Rectifying characteristics will be observed for (n^+-type Ga_2Te_3)/(*p*-type GaAs) structures, whereas this excess *n*-type (As) doping of the Ga_2Te_3 will contribute to an Ohmic-type conductivity across the Ga_2Te_3/(*n*-type GaAs) interface. Specifically, degenerate *n*-type (As) doping of thin Ge and Si layers grown on top of *n*-type GaAs, namely, was shown to result in Fermi-level unpinning at these semiconductor-semiconductor interfaces.[31,32] The (near) Ohmic-contact behavior and small barrier height observed for an abrupt highly ($\simeq 5\times 10^{19}$/cm^3) (Si-doped n^+-type InAs)/[*n*-type GaAs (1.10^{17}/cm^3)] heterojunction is explained by this mechanism.[33] As the conduction-band discontinuity [0.37 eV (Refs. 34 and 35)] and lattice mismatch (4%) at a Ga_2Te_3/GaAs interface are even smaller than at an InAs/GaAs interface [0.54 eV (Refs. 33 and 35) and 7%], a low resistive (near) Ohmic conductivity across an (n^+-type Ga_2Te_3)/(*n*-type GaAs) interface can also be expected. The observation of the Ga_2Te_3 pseudomorphic growth, and of elemental tellurium in the Ohmic-contact structures, fits equally well into this model. Due to pseudomorphic growth, the formation of dislocations and corresponding conduction-band discontinuity at the heterointerface will be reduced[3,36]; the presence of the smaller band-gap semiconductor Te ($E_g=0.33$ eV compared to 1.0 eV for Ga_2Te_3), presumably as an outermost surface layer (at least for the 500–550 °C (RTA) annealed samples), only can yield better contacting properties.

However, a most critical element in the formation of the (observed) (Au/Te)-GaAs fully Ohmic-contact structure remains the barrier reduction at the GaAs side of the junction. Two possibilities exist: either an increased Te *n*-type doping of a GaAs interface layer occurs, or a $GaTe_xAs_{1-x}$ transition layer is formed.[3] Neither of these features could be verified with the analysis techniques used in the present study. It was outlined above that the presence of a highly doped layer within the GaAs depletion region could not be excluded. A possible grading of the Ga_2Te_3/GaAs interface could not be verified either, as sputter depth profiling and AES lack the required depth resolution due to the rough interface structure. Both of these events (doping and grading), however, are likely to occur. As the formation of the Ga_2Te_3/GaAs heterostructure is driven by (Au-Ga, As, and Te) interdiffusion processes, a graded $GaTe_xAs_{1-x}$ transition layer might be present. Also for the deepest indiffused Te atoms, a dopant behavior, not exceeding the Te-GaAs equilibrium *n*-type doping limit ($\simeq 5.10^{18}$/cm^3) (Refs. 2 and 24) is plausible.

Another crucial point regarding the applicability of the (n^+-type Ga_2Te_3)/(*n*-type GaAs) Ohmic-contact model is the remaining question of how to explain the non-Ohmic behavior of the Au/Te/Au/GaAs contact structures annealed at 400 °C (RTA). Both XRD and the Mössbauer technique indicate for this alloy condition the formation of highly Au-doped Ga_2Te_3. From AES, the presence of As in this compound cannot be excluded. The clarification of the non-Ohmicity, linked with this Au-Ga_2Te_3 formation, is related to the different properties of the alloy compared to those of pure Ga_2Te_3. The solubility of Au in Ga_2Te_3 was shown to be limited to a value between 14 and 17 at. %.[30] Corresponding changes in the semiconductor structure, with most notably a lattice-constant increase by 1.3%, were indicated both by Mössbauer and XRD measurements. The band gap of the alloy increased to 1.2 eV, compared to 1.0 eV for pure Ga_2Te_3.[30] These observations can be explained by the formation of a ternary, chalcopyritelike, semiconductor which we tentatively label as $AuGa_2Te_3$. Two of the $AuGa_2Te_3$ semiconductor properties, namely, the higher band gap (decreasing its contactibility) and increased lattice constant (yielding a higher dislocation density at the $AuGa_2Te_3$/GaAs interface) might explain the non-Ohmic behavior observed for the 400 °C (RTA)-annealed Au/Te/Au/GaAs contact structures. Most striking, however, is the inability to create a clearly observable *n*-type conductivity in this $AuGa_2Te_3$ compound, even when atomic percents of As were added.[30] Thus, either arsenic does not act as an *n*-type dopant in $AuGa_2Te_3$ or, due to compensation, the free-carrier density saturates at a lower level than in Ga_2Te_3. Consistent herewith is the fact that rectifying characteristics were obtained, even when the *I-V* characteristics of only one 400 °C (100×100 μm^2) contact were probed, short circuiting in this way the metallization-substrate junction. Hence, the transition from non-Ohmic to Ohmic-behaving Au/Te-GaAs contacts, by increasing the alloy temperature from 400 to 500 °C, can most consistently be interpreted as being due to an increased formation of As-doped Ga_2Te_3 providing, as argued above, a low-resistivity conduction path from the GaAs substrate to the metal probes.

Finally, it can be pointed out that a similar model

might hold also for the Ge-based Ohmic-contact metallizations. To our viewpoint, the data reported on these Ohmic-contact structures can be argued to be more in agreement with the hypothesis of a more crucial role to be fulfilled by an As doping of the Ge top layer, than by a Ge doping of the GaAs substrate. It was shown by an analysis of *I-V* and *C-V* measurements combined with AES depth profiling,[6] and by back-side secondary-ion-mass spectroscopy (SIMS) measurements[37] that the largest reduction in r_c of alloyed Au-Ge/GaAs contact structures occurred before the Ge diffused into the GaAs substrate. Also, back-side SIMS profiling of annealed Ge/Pd/GaAs structures did not yield a clear indication for a possible Ge doping of the GaAs substrate.[2] Electrical measurements on a Ni(Ge)InW contact metallization did not support the hypothesis of a preferential Ge-dopant behavior at the metal-GaAs interface, either.[38] On the other hand, evidence for the regrowth of Ge layers on top of the GaAs substrate was found for both the Au-Ge[15] and Ge/Pd[2] contact metallizations. As yet, the presence of both Ga and As elements was detected in this Ge; the doping level and type of these layers remains to be determined.[2] However, if a dominant arsenic *n*-type doping might occur, a similar Fermi-level unpinning at the Ge/GaAs interface, as argued upon for the Ga_2Te_3/GaAs heterojunction, and formation of an Ohmic metal-Ge barrier can be expected. This approach, without intervening GaAs doping or Ge/GaAs grading, was used in the formation of an MBE-grown (n^+-type Ge)/GaAs Ohmic-contact structure.[39]

To conclude, from this investigation of furnace-alloyed Au/Te/Au/(*n*-type GaAs) Ohmic contacts, no arguments in favor of the doping or amorphous heterojunction models can be deduced. Strong evidence is found for attributing the observed low-resistive conductivity to the formation of an (n^+-type Ga_2Te_3)/(*n*-type GaAs) heterojunction, in agreement with the (graded) crystalline heterojunction model. Whether an increased doping at the GaAs side of the junction, or the formation of a graded Ga_2Te_3/GaAs transition layer takes place remains unverified. More crucial, however, is the arsenic doping of the Ga_2Te_3 top layer. A similar concept is proposed to hold for the Au-Ge and Ge/Pd contact metallizations also.

ACKNOWLEDGMENTS

The authors wish to thank G. Borghs (IMEC) for providing the MBE-grown n^+-type GaAs layers. This work was supported by the Interuniversitair Instituut voor Kernwetenschappen (IIKW) and the Instituut tot Aanmoediging van het Wetenschappelijk Onderzoek in de Nijverheid en Landbouw (IWONL). A fruitful discussion with Professor Dr. W. E. Spicer (Stanford) is gratefully acknowledged.

[1]C. J. Palmstrøm and D. V. Morgan, in *Gallium Arsenide Materials, Devices, and Circuits,* edited by M. J. Howes and D. V. Morgan (Wiley, New York, 1985), p. 195.

[2]C. J. Palmstrøm, S. A. Schwarz, E. Yablonovitch, J. P. Harbison, C. L. Schwartz, L. T. Florez, T. J. Gmitter, E. D. Marshall, and S. S. Lau, J. Appl. Phys. **67**, 334 (1990).

[3]T. Sebestyen, Solid-State Electron. **25**, 543 (1982).

[4]D. Kirillov and Y. Chung, Appl. Phys. Lett. **51**, 846 (1987).

[5]R. S. Popovic, Solid-State Electron. **21**, 1133 (1978).

[6]A. Illiadis, J. Vac. Sci. Technol. B **5**, 1340 (1987).

[7]K. Wuyts, A. Vantomme, R. E. Silverans, M. Van Hove, and M. Van Rossum, in *Advances in Materials, Processing and Devices in III-V Compound Semiconductors,* edited by D. K. Sadana, L. Eastman, and R. Dupuis, MRS Symposia Proceedings No. 144 (Materials Research Society, Pittsburgh, 1989), p. 545.

[8]K. Wuyts, G. Langouche, H. Vanderstraeten, R. E. Silverans, M. Van Hove, M. Van Rossum, H. Münder, and H. Lüth, in *Advanced Metallizations in Microelectronics,* edited by A. Katz, S. P. Muraka, and A. Appelbaum, MRS Symposia Proceedings No. 181 (Materials Research Society, Pittsburgh, 1990), p. 345.

[9]K. Wuyts, J. Watté, R. E. Silverans, M. Van Hove, and M. Van Rossum, Appl. Phys. Lett. **59**, 1779 (1991).

[10]K. Wuyts, G. Langouche, M. Van Rossum, and R. E. Silverans, Phys. Rev. B **45**, 6297 (1992).

[11]G. J. Kemerink, H. de Waard, L. Niesen, and D. O. Boerma, Hyperfine Interact. **14**, 53 (1983).

[12]H. Münder, C. Andrzejak, M. G. Berger, H. Lüth, G. Borghs, K. Wuyts, J. Watté, and R. E. Silverans, J. Appl. Phys. **71**, 739 (1992).

[13]K. Wuyts, J. Watté, R. E. Silverans, H. Bender, M. Van Hove, and M. Van Rossum, J. Vac. Sci. Technol. B **9**, 228 (1991).

[14]K. Wuyts, G. Langouche, and R. E. Silverans, Hyperfine Interact. **53**, 431 (1990).

[15]M. A. Dornath-Mohr, M. W. Cole, H. S. Lee, C. S. Wrenn, D. W. Eckart, D. C. Fox, L. Yerke, W. H. Chang, R. L. Lareau, K. A. Jones, and F. Cosandy, J. Electron. Mater. **19**, 1247 (1990).

[16]L. Lu-Min Yeh, in *Advances in Materials, Processing and Devices in III-V Compound Semiconductors* (Ref. 7), p. 607.

[17]N. Holonyak, D. L. Keune, R. D. Burnham, and C. B. Duke, Phys. Rev. Lett. **24**, 589 (1970).

[18]H. Bender, K. Wuyts, J. Watté, and R. E. Silverans, in *Proceedings of the Fourth European Conference on Applications of Surface and Interface Analysis, Budapest, 1991* [Surf. Interf. Anal. (to be published)].

[19]J. Vanhellemont (private communication).

[20]P. Boolchand, W. Bresser, and G. J. Ehrhart, Phys. Rev. B **23**, 3669 (1981).

[21]G. Langouche, B. Hlimi, O. El Hajjaji, G. Marest, I. Berkes, M. Van Der Heyden, and M. Tong, Hyperfine Interact. **28**, 849 (1986).

[22]G. Langouche, D. Schroyen, H. Bemelmans, M. de Potter, W. Deraedt, and M. Van Rossum, in *Defects in Electronic Materials,* edited by M. Stavola, S. J. Pearton, and G. Davies, MRS Symposia Proceedings No. 104 (Materials Research Society, Pittsburgh, 1988), p. 527.

[23]J. C. Woolley, and B. A. Smith, Proc. Phys. Soc. London **72**, 867 (1958).

[24]G. Borghs (private communication).

[25]G. Abstreiter, E. Bauser, A. Fisher, and K. Ploog, Appl. Phys.

16, 345 (1978).
[26]G. Burns, F. H. Dacol, C. R. Wie, E. Burnstein, and M. Cardona, Solid State Commun. **62**, 449 (1987).
[27]D. C. Look, *Electrical Characterization of GaAs Materials and Devices* (Wiley, Chichester, 1989) p. 45.
[28]T. Kim and D. L. Chung, J. Vac. Sci. Technol. B **4**, 762 (1986).
[29]V. G. Weizer and N. S. Fatemi, J. Appl. Phys. **64**, 4618 (1988).
[30]K. Wuyts, J. Watté, G. Langouche, R. E. Silverans, G. Zégbé, and J. C. Jumas, J. Appl. Phys. **71**, 744 (1992).
[31]J. R. Waldrop and R. W. Grant, Appl. Phys. Lett. **50**, 250 (1987).
[32]J. C. Costa, F. Williamson, T. J. Miller, K. Beyzavi, M. I. Nathan, D. S. L. Mui, S. Strite, and H. Morkoç, Appl. Phys. Lett. **58**, 382 (1991).
[33]S. L. Wright, R. F. Marks, S. Tiwari, T. N. Jackson, and H. Baratte, Appl. Phys. Lett. **49**, 1545 (1986).
[34]G. Guizetti and F. Meloni, Il Nuovo Cimento D **1**, 503 (1982).
[35]W. Pollard, J. Appl. Phys. **69**, 3154 (1991).
[36]J. M. Woodall, G. D. Petit, T. N. Jackson, C. Lanza, K. L. Kavanagh, and J. W. Mayer, Phys. Rev. Lett. **51**, 1783 (1983).
[37]R. A. Bruce, D. Clarke, and S. Eickenz, J. Electron. Mater. **19**, 225 (1990).
[38]M. Murakami, W. H. Price, M. Norcott, and P. E. Hallali, J. Appl. Phys. **68**, 2468 (1990).
[39]R. A. Stall, C. E. C. Wood, K. Board, N. Dandekar, L. F. Eastman, and J. Devlin, J. Appl. Phys. **52**, 4062 (1981).

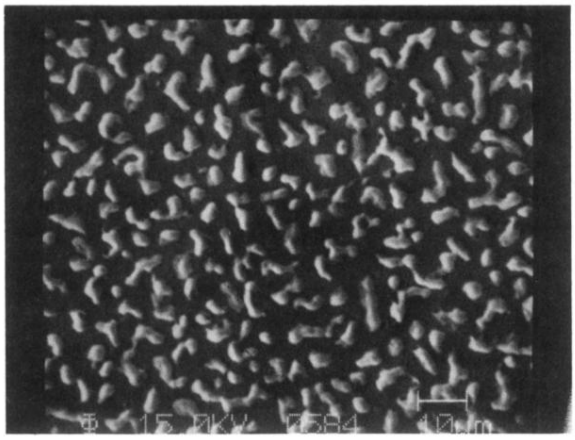

FIG. 1. SEM micrograph of the surface of a (1200-Å Au)/(500-Å Te)/(50-Å Au)/GaAs sample alloyed at 500 °C. The marker denotes a length of 10 μm.